


Adsorption Behavior of Methylene Blue Onto Activated Coconut Shells: Kinetic, Thermodynamic, Mechanism and Regeneration of the Adsorbent

Dose-Response:
An International Journal
October-December 2024:1–18
© The Author(s) 2024
Article reuse guidelines:
sagepub.com/journals-permissions
DOI: 10.1177/15593258241290708
journals.sagepub.com/home/dos


Moussa Abbas¹  and Mohamed Trari²

Abstract

Adsorption techniques are widely used to remove some classes of pollutants from waters, especially those which are not easily biodegradable. The removal of Methylene blue (MB), as a pollutant, from waste waters of textile, paper, printing and other industries has been addressed by the researchers. The aim of this study is to eliminate MB by Activated Coconut Shells (ACS) produced at low cost by adsorption in batch mode. The ACS was characterized by the FTIR spectroscopy and point of zero charge (pHpzc: 5.06). Some examined factors were found to have significant impacts on the MB uptake of ACS like the initial dye concentration C_0 (40-120 mg/L), solution pH (2-8), ACS dose (1-12 g/L), agitation speed (50-500 r/min), particles size (1.0-1.2 mm) and temperature (298-333 K). The best capacity was found at pH 6 with an adsorbent dose 8 g/L, an agitation speed 200 r/min and a contact time of 60 min. Modeling Kinetics and Isotherms shows that the pseudo-second-order kinetic model with R^2 (0.935 -0.998) and Langmuir adsorption isotherm model provide better fitness to the experimental data with the maximum adsorption capacity of 30.30 mg/g at 25°C. The separation factor R_L (0.933-0.541) in the concentration range studied (10-120 mg/L) shows a favorable adsorption. The isotherms at different temperatures have been used for the determination of the free energy ΔG° (198-9.72 kJ/mol); enthalpy ΔH° (82.082 kJ/mol) and entropy ΔS° (245.689 J/K mol) to predict the nature of MB adsorption process. The positive values of (ΔG°) and (ΔH°) indicate a non-spontaneous and endothermic MB adsorption with a chemisorption. The adsorbent elaborated from Coconut Shells was found to efficient and suitable for the removal of MB dye from aqueous solutions, due to its availability, low cost preparation and good uptake capacity.

Keywords

adsorption, kinetics, modeling, thermodynamic, Methylene blue, coconut Schell

Introduction

Water contamination by dyes can lead to various environmental problems. Colored water can affect plant life and thus an entire ecosystem can be destroyed by contamination of various dyes in water.¹ Although MB is used in some medical applications, it can also be used in textile, leather, food processing, dyeing, cosmetics, paper, dye manufacturing and printing. With the increasing focus on environmentally friendly industry, it is important to move towards the low-cost and effective methods for wastewater treatment. MB causes eye burns, which can be responsible for permanent damage and can cause several health hazards, such as nervous system

¹ Laboratory of Applied Chemistry and Materials (LabCAM), University of M'hamed Bougara of Boumerdes, Avenue de l'Indépendance, Boumerdes, Algeria

² Laboratory of Storage and Valorization of Renewable Energies, Faculty of Chemistry (USTHB), Algiers, Algeria

Received 1 July 2024; accepted 20 September 2024

Corresponding Author:

Moussa Abbas, Laboratory of Applied Chemistry and Materials (LabCAM), University of M'hamed Bougara of Boumerdes, Avenue de l'Indépendance, Boumerdes 35000, Algeria.

Emails: m.abbas@univ-boumerdes.dz; moussaiap@gmail.com



Creative Commons Non Commercial CC BY-NC: This article is distributed under the terms of the Creative Commons Attribution-NonCommercial 4.0 License (<https://creativecommons.org/licenses/by-nc/4.0/>) which permits non-commercial use, reproduction and distribution of the work without further permission provided the original work is attributed as specified on the SAGE

and Open Access pages (<https://us.sagepub.com/en-us/nam/open-access-at-sage>).

and liver damage when ingested. Therefore, the treatment of effluents containing this dye is of interest because of its aesthetic impacts on receiving waters. The presence of dyes in water increases the chemical and biochemical oxygen demand. The global demand for water and the amount of wastewater produced continues to increase, creating an urgent need for purification methods. Wastewater is often discharged into rivers and lakes or seeps into aquifers, significantly affecting freshwater quality. Globally, more than 80% of wastewater returns to the environment untreated with negative consequences for the marine environment.² Indeed, A about 600 organic and inorganic pollutants has been listed in water along with biological species.³ The presence of dyes, even in low concentrations, weakens the penetration of light through the water surface, significantly inhibiting the photosynthetic process of aquatic flora, according to the Beer-Lambert law. Currently, there are about 10 000 types of synthetic dyes with a global production of 7×10^5 tons per year.⁴ MB is a cationic dye appears as a green crystalline powder, highly soluble in water. MB is a cationic dye that comes in the form of a green crystalline powder, highly soluble in water. It is used for dyeing cotton, paper, silk, wood and leather products.⁵ Therefore, many treatments were applied to limit the its concentration in aqueous medium like adsorption,⁶⁻¹⁴ biological treatment,¹⁵ detoxification,¹⁶ photo catalysis^{17,18} and electrochemical degradation.¹⁹ Adsorption is attractive for the removal of pollutants because of its low cost, simplicity of design, removal efficiency, and ease of use and availability of materials. In this respect, agricultural wastes have advantages as adsorbents, they are readily available, cost-effectiveness, renewable, require less processing time, with an uptake capability and can be easily regenerated. They can be modified by treating it with chemical agents, alkalis, acids, organic compounds, *etc.*, or thermally, this modification could have beneficial effects on chemical/physical properties like increasing surface area, improved pore structure and functional group. This has prompted a growing research interest in the production of activated carbons from renewable and cheaper precursors which are either industrial or agricultural by-products, for the water treatment. Modified carbons exhibit adsorption capacity with selectivity and sensitivity.²⁰ In this optic, agricultural wastes such as cotton stalk,² olive stones,²¹ coconut shell,²² rice husk,²³ orange peel,⁶ pistachio shell²⁴ wheat bran²⁵ titanium dioxide²⁶ mesoporous silicate.²⁷ Modified Tetra selmis sp,²⁸ hybrid polymer²⁹ and Chitosan^{30,31} are used in recent years for their availability. The aim of this study is to eliminate Methylene blue by adsorption on Activated Coconut Shells (ACS), produced at low cost by adsorption in batch mode. The characteristic of ACS was investigated and the influences of operational parameters namely pH, adsorbent dose, contact time, temperature, particle size and initial dye concentration were also reported. The equilibrium adsorption data were fitted to various equations to obtain the constants related to the MB elimination. Finally, this study focuses on the important points, namely the synthesis of

low-cost activated carbon from waste and its valorization in water treatment. This is in order to contribute to the reduction of environmental pollution which remains a global problem, to move from batch mode to column mode, to carry out tests on a semi-pilot scale and to carry out theoretical simulations of adsorption phenomena. The tests of homogeneous photo-degradation of the dye on the TiO₂ semiconductor will be a logical continuation of this study in the near future.

Materials and Methods

The spectrophotometry is a technique which owes its development to progress in the quantum mechanics allowing, among other things, to identify a chemical substance and to determine the concentration in solution. Two light sources were used: a visible tungsten halogen lamp and a UV deuterium lamp; the scanning speed was set at 1200 nm min⁻¹. Blanks were performed in a quartz cell (10 mm) and calibrated with ultrapure water. Residual concentration measurements were obtained by linear interpolation from a calibration graph. The pH of the solutions was accurately measured with a microprocessor-based pH meter of the HANNA HI 8521 type, calibrated with commercial buffers of pH 4, and 10. The pH was adjusted to by using H₂SO₄ and NaOH obtained from Sigma - Aldrich Company (respectively for acidic and basic media).

The FT-IR spectroscopy was used to identify the functional groups of ACS. 5 mg of adsorbent were mixed with dry KBr (Extra pure) of spectroscopy quality and pressed under 4 kbar to form thin pellet. Then, the FTIR spectra were plotted with a Perkin Elmer 2000 infrared spectrometer in the range (4000-400 cm⁻¹) for 16 times to increase the "signal / noise" ratio.

The Zero Point Charge (pH_{ZPC}) of the adsorbent, ie, the pH for which the surface charge is zero, is obtained using a procedure reported elsewhere.³² 20 mL of KNO₃ (99.40%) solutions (0.01 M) were placed in closed conical flasks; the pH of each solution was adjusted between 2 and 14 by addition of HCl (37%) or NaOH (97%) solution. Then, 0.1 g of adsorbent was added to each solution and the final pH was measured after 24 h under magnetic stirring at 25°C; pH_{ZPC} is the point of intersection of the final pH and initial pH lines.

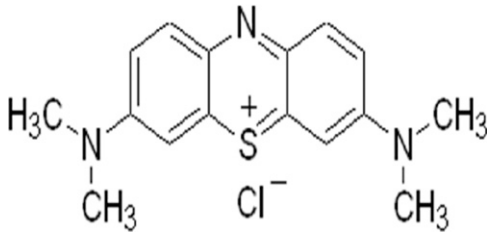
Methylene Blue Adsorbate

Methylene Blue (99.98 %) is a Basic Blue 9 dye, whose IUPAC name is 3,7-bis (dimethylamino) phenothiazin-5-ium chloride, C.I. 52015, with a chemical formula C₁₆H₁₈CIN₃S (MW = 319.85 g/mol); the absorbance peaks (λ_{max} = 662 nm). Chemical structure and properties of MB are summarized in Table 1.

Preparation of Adsorbent

Almond shell is the lignocellulosic material forming the thick endocarp of the almond fruit and represents more than 50% of

Table I. Methylene Blue Properties.

Properties		Structural formula
Brute formula	$C_{16}H_{18}ClN_3S$	
Molecular weight (g/mol)	319.85	
Composition (%)	C: 60.08, H:5.67,S: 10.03 N: 13.14, Cl: 11.08	
Wavenumber λ_{max} (nm)	662	
Name basic blue 9	Cl 52015	
Melting temperature	180°C	
Solubility in water (g/L)	40 at T = 20°C	
Solubility in alcohol (g/L)	10 at T = 20°C	

the total weight of the seed and constitutes a significant percentage as raw material used for the preparation of activated carbons. The shells obtained are washed thoroughly with distilled water to remove any kind of dust or adhering impurities until clear washing water was obtained. The material was dried at 110°C (24 h) to avoid possible alteration of the physicochemical properties of the material. Several researchers have practiced moderate drying of the biosorbent, in particular using solar energy. The particle sizes used for the adsorption tests were isolated mechanically by means of a sieve whose mesh size corresponds to diameters [0.71-0.22 mm], and the samples were stored in bottles. Pyrolysis is necessary to transform the raw material; the carbonaceous raw materials are very characteristic with an infinite number of pores clogged by organic matter. This carbonaceous material must be freed from all these organic products. To do this, it is heated to a high temperature of 700°C in a rotary kiln. After washing and drying, part of the material is subjected to a heat treatment. The material is carbonized at a temperature of 700°C (5°/min., 1 h. This process gives a carbon with narrow pores and generates microscopic alveoli on the surface of the carbon, thus increasing its active surface and its adsorption power.

Adsorption Experiment

The effects of the initial MB concentration (C_0 :40-120 mg/L), pH (2-8), adsorbent dosage(1-12 g/L), stirring speed (50 - 500 r/min) and temperature (20-60°C) on the MB adsorption was investigated in batch mode for a specific contact time (0-60 min). The MB solutions were prepared by dissolving the accurate amount MB (99 %) in distilled water, used as a stock solution and diluted to the required initial concentrations. Adsorption was carried out at room temperature under atmospheric pressure. It was performed by introducing a mass of adsorbent into a glass Erlenmeyer (100 mL capacity), containing 100 mL of an aqueous solution of determined concentration. The mixture was magnetically stirred at 150 r/min for a fixed time.

Then, separation was performed by centrifugation (6000 r/min, 5 min) and the suspension was analyzed by UV-Visible

spectroscopy ($\lambda_{max} = 662$ nm) to determine the residual concentration of MB. The amount q_t (mg/g) yield R (%) of adsorbed MB (q_i) was calculated from the relations:

$$q_t = \frac{(C_0 - C_t) \cdot V}{m} \quad (1)$$

$$R_t(\%) = \frac{(C_0 - C_t) \cdot 100}{C_0} \quad (2)$$

Where C_0 is the initial MB concentration and C_t the concentrations (mg/L) at time t, V the volume of solution (L) and m the mass of ACS (g).

To confirm the correlation, a statistical error calculation is essential, among the most used error functions are the following. Due to the inherent bias resulting from linearization of the isotherm and kinetic models, for non-linear regression, the determination coefficient (R^2) is insufficient for evaluating the fit goodness, thus, the error models, Chi-Squares (X^2) test equation is used as criteria for the fitting quality:

$$X^2 = \sum_1^N \frac{(q_{e,exp} - q_{e,cal})^2}{q_{e,cal}} \quad (3)$$

Where, $q_{e(exp)}$ (mg/g) is the experimental value of uptake, $q_{e(cal)}$ the calculated value using a model (mg/g) and N the number of observations in the experiment (the number of data points); the smaller X^2 value indicates the better curve fitting.

Results and Discussion

Characterization of Adsorbent

Figure 1 shows that the FT-IR spectra have similar profiles, but with different band intensities. A broad band at around 3420 cm^{-1} corresponding to the elongation of O-H groups, the wide band at 2926 cm^{-1} is related to the elongation of C-H group, the band at 1739 cm^{-1} corresponding to the C = O group while that band at 1605 cm^{-1} is characteristic of the elongations of C = C bonds of olefins and aromatics, the band located at 1383 cm^{-1} is linked to the C-H deformations in the aliphatic chains whereas that centered at 1045 cm^{-1}

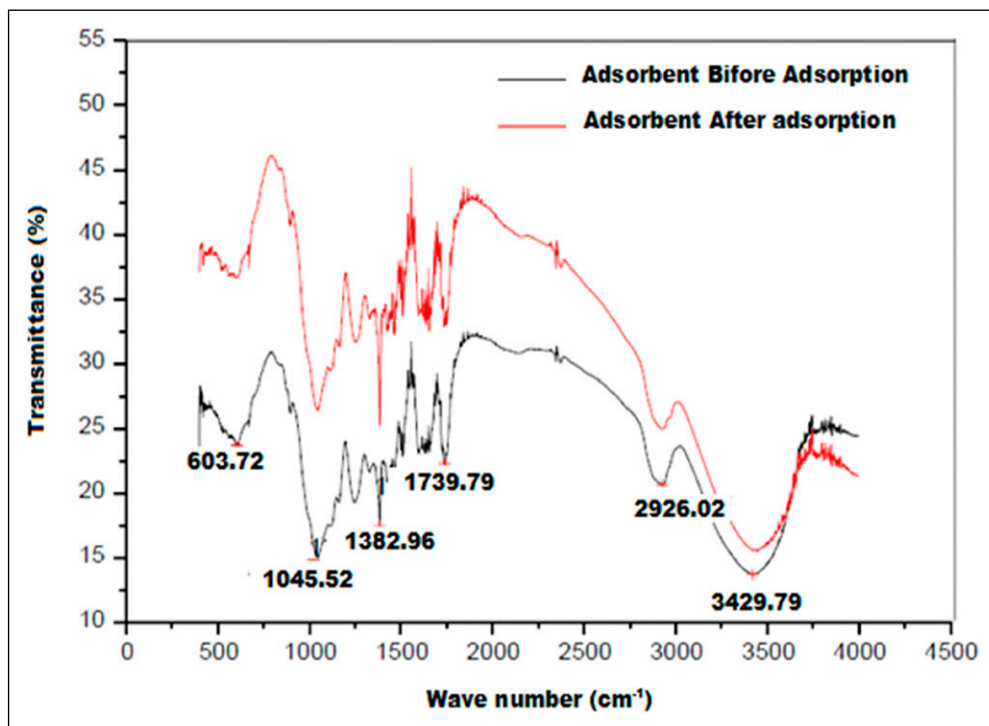


Figure 1. FTIR spectra for Activated Coconut shell (ACS).

characteristic of the deformation in the plane of Aliphatic C-O. These bands result from the presence of cellulose, hemicelluloses and lignin, major constituents of coconut shell.

Analyses of the ACS Surface Morphology

The SEM micrographs of ACS before and after adsorption are shown in [Figure 2](#); the prepared ACS presents a microporous structure with different pore diameters and a rough surface and many protrusions. The higher magnification shows that the adsorbent surface contains a considerable number of pores with a high probability that MB molecules are adsorbed. After adsorption, the ACS surface became smoother where the roughness was considerably reduced with less visible pores, indicating a clear adsorption on both the surface and in pores. The images also reveal that the exterior surfaces of the ACS are filled with inhomogeneous cavities of different sizes and shapes. These cavities differ from carbon to carbon in the reaction of the activating agent; they are the external pores which represent the main channels for accessing to internal surface (micropores and mesopores) of the activated carbon.

Influence of contact time and MB concentration of on the adsorption capacity

MB concentrations and the adsorbent dose are important factors for adsorption. To demonstrate the effect of the initial concentration (C_0), experiments were performed in the range

C_0 (40-120 mg/L) and ACS dose of 5g/L. The temperature was kept constant at 25°C and the mixture was stirred at 200 r/min. Samples were collected at regular time intervals, centrifuged and analyzed spectrophotometrically.

[Figure 3](#) shows a very rapid adsorption, where a saturation level is reached after 60 min.; the latter indicates the formation of a monolayer. It is noted that the adsorption capacity increases with C_0 ; this is due to the fact that the diffusion of MB molecules towards the surface of the adsorbent is accelerated by the concentration gradient according to the diffusion law; a similar result has already been obtained for the adsorption of MB on apricot kernels.²³ By increasing the concentration C_0 (40 - 120 mg/L), the MB removal efficiency decreases from (79 to 41%) and it can be deduced that the adsorption of MB on ACS occurs in three stages:

- (i) *In range (0-20 min)* fast adsorption of MB due to the presence of free sites on the adsorbent surface which translates the linear increase of the adsorption capacity over time.
- (ii) *In range (20-50 min)* reduction of the adsorption rate, reflected by a small increase in the adsorption capacity attributed to the decrease in the quantity of MB in solution and the number of available unoccupied sites.
- (iii) *In range (50-60 min)* stability of the adsorption capacity is observed, due to the complete occupation of adsorption sites: the establishment of the stable level therefore reflects this stage. The adsorption capacity

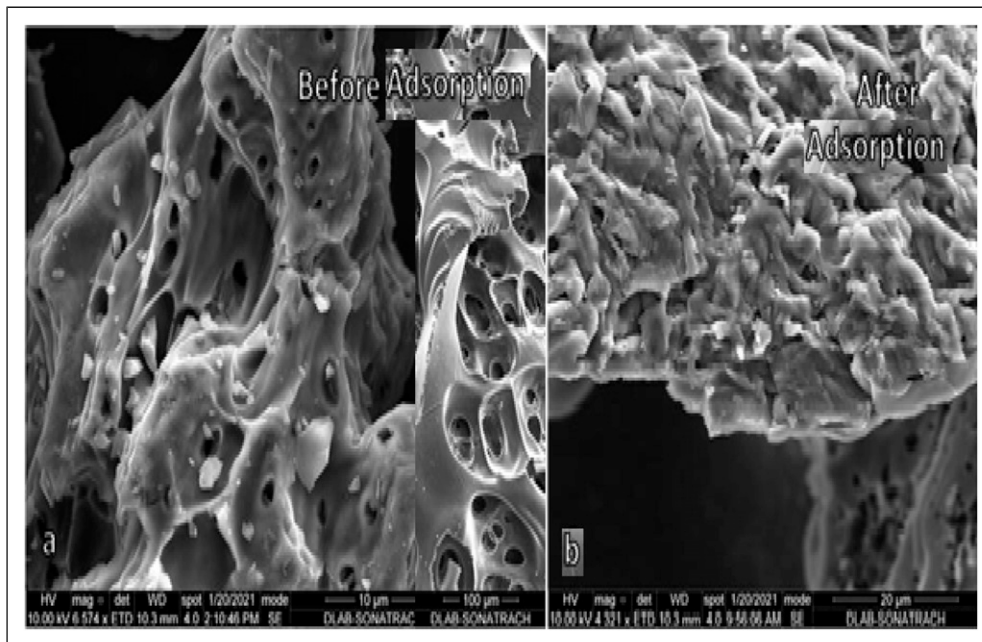


Figure 2. Microscopic images of the adsorbent (ACS): (a) Before adsorption of MB (b) After adsorption of MB.

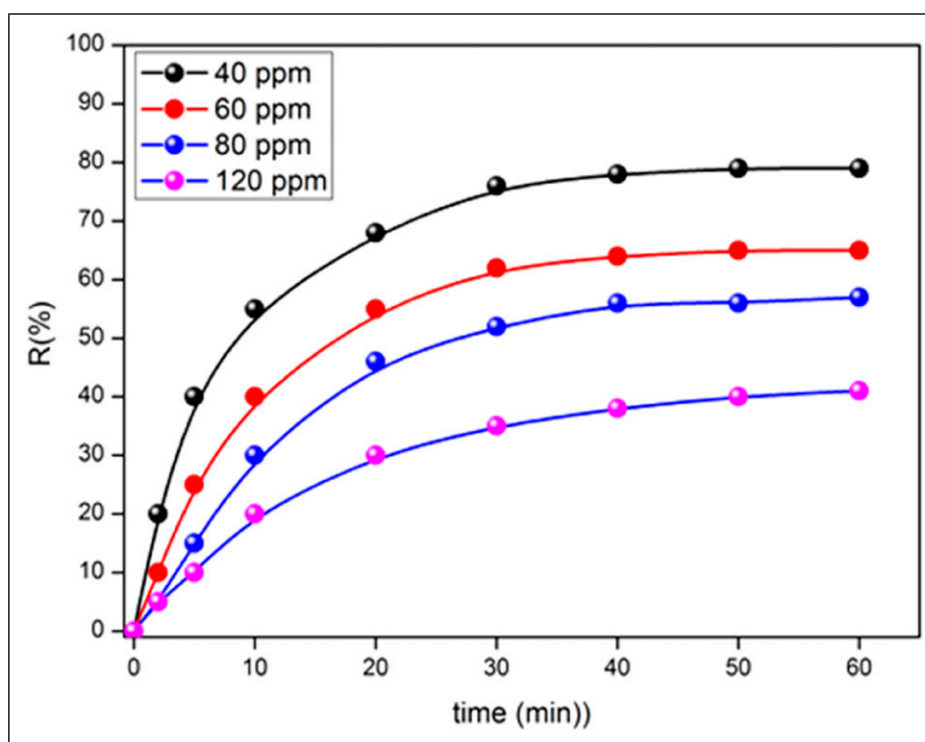


Figure 3. Effect of contact time and concentration on the adsorption of MB onto ACS: (Adsorbent dose: 5 g/L, Co: (40-120 ppm), Particle size: 0.2 mm, pH: 6, Agitation speed: 200 r/min, and T: 25°C).

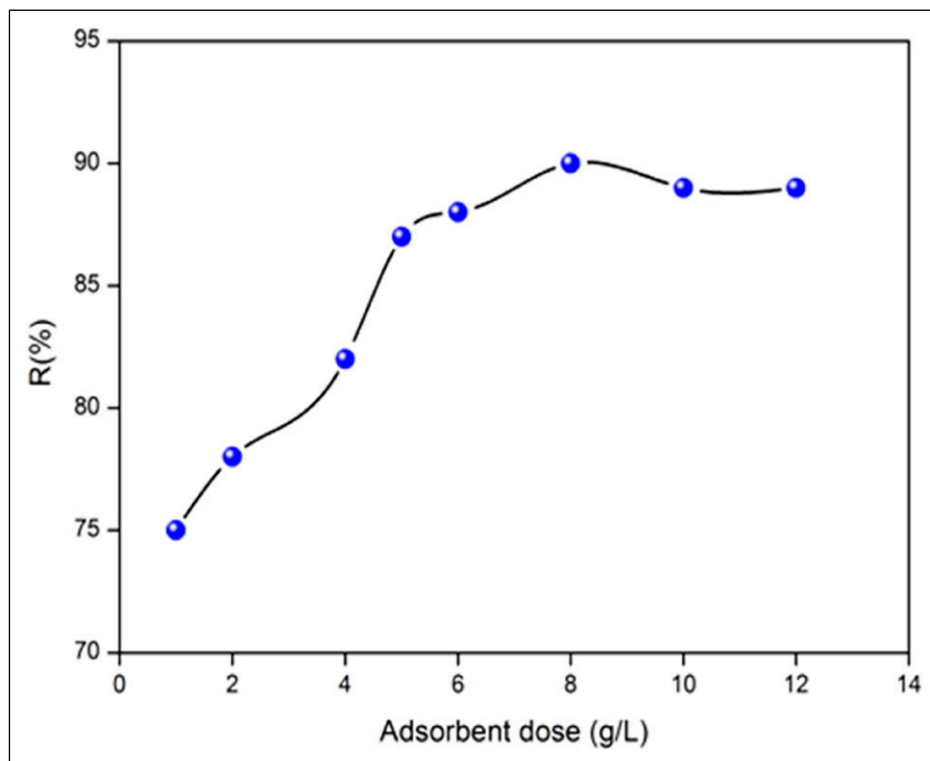


Figure 4. Effect of adsorbent dose on the adsorption of MB onto ACS: ($C_o = 10$ ppm, Particle size: 0.2 mm, pH = 6, Agitation speed: 200 r/min, time 60 min, and $T = 25^\circ\text{C}$).

of MB increases over time to reach a maximum after 60 min. and thereafter tends toward a constant value indicating that no more MB are removed from the solution.

Influence of adsorbent dosage

Determination of the minimum mass of a material required to adsorb a given pollutant is an essential step in adsorption. We started this step on the removal of MB and to evaluate the optimal ACS content, test experiments were performed on a MB solution (10 mg/L), to which different amounts of adsorbent were added in the range (1 - 12 g/L). The variations of the amount of MB adsorbed during the contact time, as a function of the ACS dose, are illustrated in Figure 4. As expected, the amount of MB adsorbed increases in the range (1 - 8 g/L), due to the number of available sites that increases with the amount of ACS and decreases in the region (9 - 12 g/L), where the number of sites becomes stable^{33,34}; this behavior can be explained by:

- (i) As long as the amount of adsorbent added to the MB solution is low, the MB molecules can easily access the adsorption sites. The addition of adsorbent increases the number of available sites but the dye charges, depending on its functional groups, have difficulty approaching these sites due to steric

hindrance (the electrical state of the surface of the adsorbent with the dye);

- (ii) A large amount of adsorbent promotes particle agglomeration, resulting in a reduction of the active adsorption surface and a decrease in the amount of adsorbate per unit mass of adsorbent. Therefore, an adsorbent dose of 8 g/L was selected for subsequent experiments.

Influence of pH

Adsorption is a surface phenomenon, which depends on the morphology of the adsorbent and is linked to the net charge on the surface. The latter is conditioned by the nature of the functional groups present, which are a combination of positive and negative groups. Indeed, at low pHs, the predominance of H^+ ions in solution favors the neutralization of negative surface charges and the total charge is dominant and positive. On the other hand, at basic pH the surface charge is negative. Monitoring the evolution of the surface charge shows that it passes through a state of neutrality, the corresponding state of which is known as the zero point charge (pHpzc). Indeed, pHpzc represents the boundary where the surface charge is zero and changes sign. ACS has pHpzc of 5.06 Figure 5.³⁵ At low pH, ACS is characterized by an anion exchange capacity: The addition of H^+ cations generates a positive charge, the anions in solution are therefore more attracted to this surface,

which slows down adsorption.³⁶ At alkaline pH, a cation exchange capacity develops: OH⁻ ions bind more and a negative charge develops, where the cations in solution are attracted to the surface. Figure 6 shows the evolution of the amount of MB adsorbed as a function of pH and reached with an optimum value at pH 6.

Effect of Agitation Speed on the Adsorption of MB

The effect of the stirring speed (50-500 r/min) on the adsorption capacity of MB onto ACS is also investigated. The optimal uptake capacity is obtained for a speed of 200 r/min (Figure 7) which gives the best homogeneity of the mixture suspension. Therefore, a speed of 200 r/min was selected for further experiments.

Influence of Particles Size

In the first stage of the batch adsorption experiments, the effect of the particle size on the MB adsorption onto ACS is examined. Significant variations in the MB uptake capacity and removal efficiency are observed for different particles sizes (0.2-1.20 mm); Figure 8 shows that the best performance is obtained for smaller sizes (0.20 mm). In general, smaller particles provide large surface areas, thus resulting in high MB uptake performance and removal efficiency. Therefore, the class 0.2 mm was subsequently used in all other adsorption experiments.

Sorption Kinetic Models

Adsorption kinetics is crucial for the design of the adsorption systems, which determines the time required to reach the steady state and many models describing the diffusion of solutes on the surface and in the pores of the adsorbent have been developed. Pseudo-first-order, pseudo-second-order, Elovich, and intraparticle diffusion are used to examine the adsorption rates of MB on ACS.

Pseudo-first-order model: It is based on the assumption that the absorption rate is directly proportional to the gradient, ie, of concentrations.³⁷ This model is generally applicable to the initial stage of an adsorption process and the nonlinear form of the model is given by the following equation:

$$\log(q_e - q_t) = \log q_e - \frac{K_1}{2.303} \cdot t \quad (4)$$

Where q_e (mg/g) and q_t (mg/g) are the amounts of the amount adsorbed at equilibrium and at time t ; k_1 (min^{-1}) the rate constant in the pseudo-first-order model determined by plotting $\text{Log}(q_e - q_t)$ vs t .

The pseudo-second-order model: This kinetic model, proposed by Ho and McKay,³⁸ assumes that the rate-limiting step is the chemisorption, where electron sharing or exchange occurs between the solute and the sorbent. This involves the adsorption of an adsorbate molecule onto two active sites on the sorbent surface where the nonlinear form of the model is given:

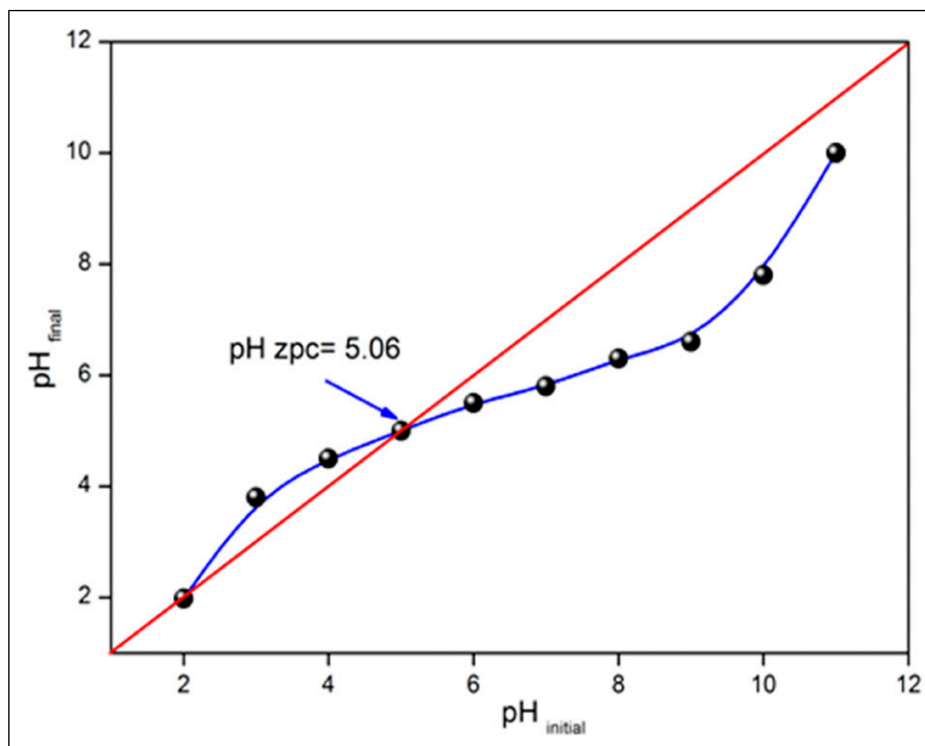


Figure 5. Determination of load predominance zones (pHzpc).

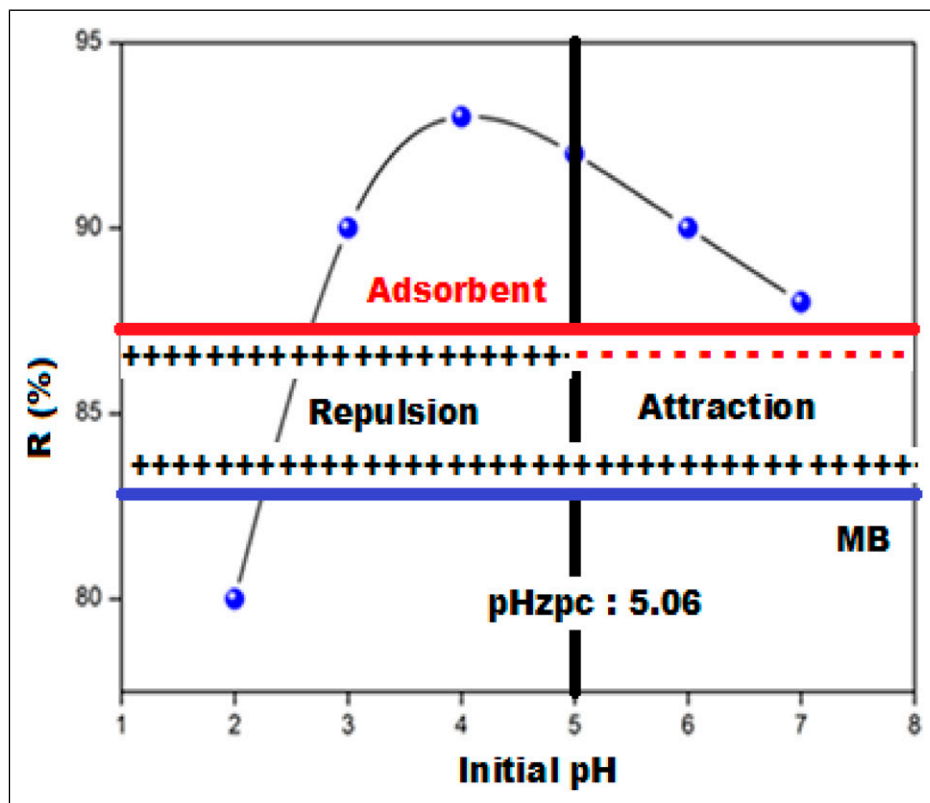


Figure 6. Effect of pH on the adsorption of MB onto ACS (Adsorbent dose: 8 g/L, Co: 10 mg/L, Particle size: 0.2 mm, Agitation speed: 200 r/min, time: 60 min, and T: 25°C).

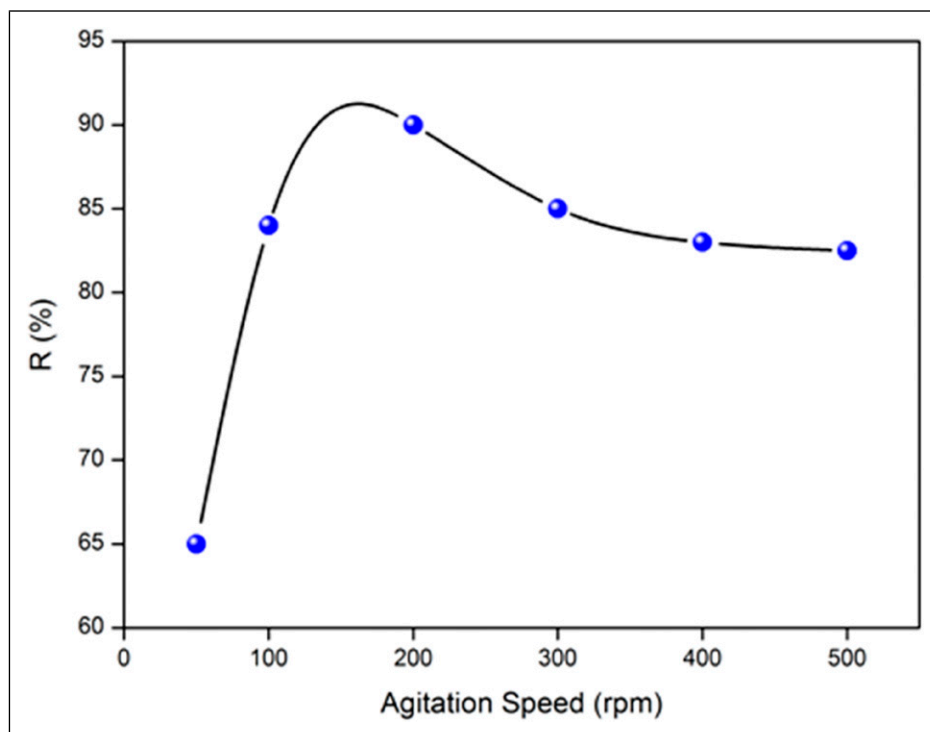


Figure 7. Effect of agitation speed on the adsorption of MB onto ACS: (Adsorbent dose: 8 g/L, Co: 10 mg/L, Particle size: 0.2 mm, pH: 6, time: 60 min, and T: 25°C).

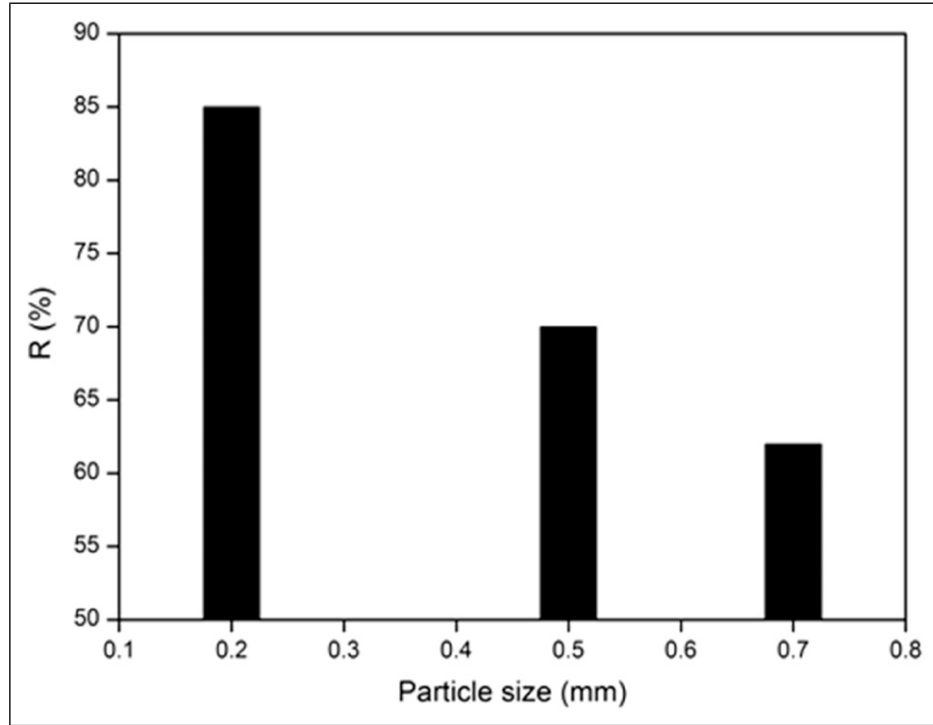


Figure 8. Effect of particles size on the adsorption of MB onto ACS: (Adsorbent dose: 8 g/L, Co: 10 mg/L, pH: 6, Agitation speed: 200 r/min, time: 60 min, and T: 25°C).

$$\frac{t}{q_t} = \frac{1}{K_2 \cdot q_e^2} + \frac{1}{q_e} \cdot t \quad (5)$$

Where k_2 (g/mg min) is the pseudo second order rate constant; q_e is determined by plotting t/q_t vs t

The Elovich model: It is used to interpret adsorption kinetics and successfully describes second-order kinetics assuming an energetically heterogeneous surface³⁹:

$$q_t = \left(\frac{1}{\beta}\right) \ln \alpha \cdot \beta + \left(\frac{1}{\beta}\right) \ln t \quad (6)$$

Where α (mg/g min) is the initial adsorption rate and β (mg/g) relates the degree of surface coverage to the activation energy involved in chemisorption.

The Intraparticle diffusion model: To identify the diffusion mechanism in adsorption, the intraparticle mass transfer diffusion model was suggested by Weber and Morris⁴⁰:

$$q_t = K_{in} \sqrt{t} + C \quad (7)$$

Where K_{in} is the intra-particle diffusion rate (mg/gmin^{1/2}), q_t the amount of MB adsorbed at time t and C (mg/g) the intercept. The constants of the different kinetic models as well as the calculation of the statistical errors obtained after modeling are grouped in [Table 2](#).

The relationship between q_t and $t^{1/2}$ shows a multilinear curve of the experimental MB data, which reflects different types of diffusion.

- (i) The first step explains the external mass transfer of dissolved MB to the outer surface of ACS.
- (ii) The second and last stages reflect the porous diffusion and equilibrium phases, respectively.

Therefore, MB adsorption is driven by more than one mechanism, ie, both chemical reaction and pore diffusion processes are involved in the iodine uptake by the adsorbent. If intraparticle diffusion occurs, then the plot q_t vs $t^{1/2}$ is linear and passes through the origin, indicating that intraparticle diffusion is the only parameter controlling the process. Otherwise, other mechanisms are also involved. The intersection gives an indication of the boundary layer thickness; the greater this, the greater the boundary layer effect.

Adsorption Equilibrium Isotherms

Adsorption isotherms that describe how an adsorbate interacts with the adsorbent are essential for adsorption optimization. The amount of adsorbate per unit mass of adsorbent at equilibrium, q_e (mg/g) and the equilibrium adsorbate concentration, C_e (mg/L) are used to plot the adsorption isotherm, q_e as a function of C_e ([Figure 9](#)). Mathematical models are used to describe the adsorption. The experimental data were fitted by four models: Langmuir, Freundlich, Temkin and Elovich that describe the solid-liquid sorption of MB on ACS.

*Langmuir model*⁴¹ postulates the occurrence of monolayer adsorption on a fixed number of localized sites. The model

Table 2. Constants of Kinetic Models (Adsorbent Dose: 5 g/L, Co: (10 -120 ppm), Particle Size: 0.2 mm, pH: 6, Agitation Speed: 200 r/min, and T: 25°C).

C _o (mg/L)	Second		Order		K ₂ (g/mg.mn)	First		K ₁ (mn ⁻¹)
	Q _{ex} (mg/g)	Q _{cal} (mg/g)	R ²	R ²		Q _{cal} (mg/g)	R ²	
40	6.324	7.092	0.998		0.0237	9.771	0.927	0.0299
60	7.82	9.524	0.991		0.0099	7.482	0.903	0.00305
80	9.125	13.157	0.935		0.0036	5.491	0.745	0.0276
120	9.845	13.951	0.995		0.0039	5.243	0.715	0.0299

C _o (mg/L)	Elovich			Diffusion			
	R ²	β (g/mg)	α (mg/g.mn)	C _o (mg/L)	K _{in} mg/gmn ^{1/2}	R ²	C (mg/g)
40	0.802	0.435	1.058	40	1.267	0.975	0.066
60	0.745	0.598	1.062	60	1.552	0.972	-0.385
80	0.595	0.886	1.756	80	1.727	0.9	-0.827
120	0.765	0.835	1.287	120	1.667	0.947	-0.644

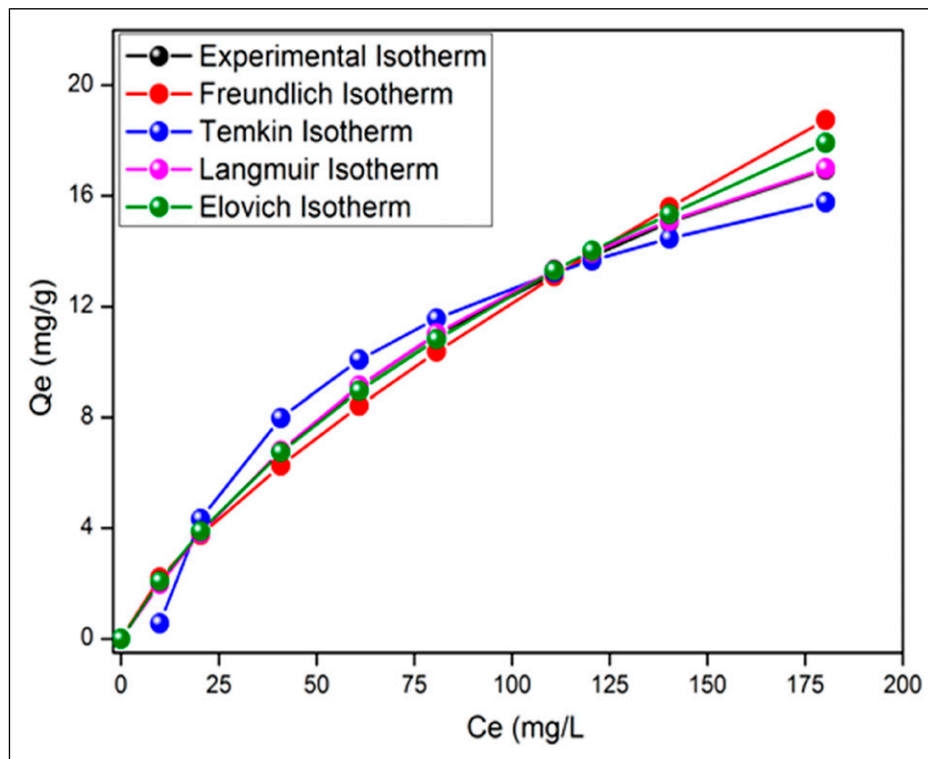


Figure 9. adsorption Isotherm of MB onto ACS in the optimum condition (Adsorbent dose: 8 g/L, Particle size: 0.2 mm, pH: 6, Agitation speed: 200 r/min, time: 60 min, and T: 25°C).

assumes that a given adsorbent surface is composed of sites equivalent in their enthalpies but without additional motion and without interactions of the adsorbed molecules; the linear expression is given by

$$\frac{1}{q_e} = \frac{1}{q_m} + \frac{1}{q_m \cdot K_L \cdot C_e} \quad (8)$$

$$R_L = \frac{1}{(1 + K_L C_0)} \quad (9)$$

The type of isotherm is indicated by the R_L value: ($R_L = 0$): irreversible, ($0 < R_L < 1$): favourable, ($R_L = 1$): linear, ($R_L > 1$): unfavourable.

*Freundlich's model*⁴² is based on the formation of multi layers of adsorbed species on a heterogeneous surface. The

enthalpies have a logarithmic distribution where the energy sites with high affinity for the adsorbate are occupied first, followed by the lower energy sites. The sorption process is summed over all sites and the linear expression of the model is given by:

$$\ln q_e = \ln K_F + \frac{1}{n} \ln C_e \quad (10)$$

K_F (L/g) and n are constants, related respectively to the capacity and favorability of adsorption extracted from the plot $\ln q_e$ vs $\ln C_e$. When n is between 2 and 10, favorable adsorption is expected, while values less than unity indicates rather poor sorption characteristics.

*Temkin's model*⁴³ postulates the heterogeneity of an adsorbent surface, whose adsorption energy distribution is linear

$$q_e = B_T \ln C_e + B_T \ln A \quad (11)$$

$$B_T = \frac{q_m \cdot R \cdot T}{\Delta Q} \quad (12)$$

ΔQ ($\frac{J}{mol}$) is the adsorption energy change and q_{max} (mg/g) the maximum adsorption capacity. The adsorption data are analyzed according to the linear plot q_e vs $\ln C_e$, enabling to calculate the constants A_T and B_T .

*Elovich model*⁴⁴ assumes that the number of adsorption sites augments exponentially with the adsorption, thus implying a multilayer adsorption:

$$\ln \frac{q_e}{C_e} = \ln(K_E \cdot q_m) - \frac{q_e}{q_m} \quad (13)$$

Where K_E (L/mg) is a constant, q_{max} (mg/g) the maximum adsorption capacity, q_e (mg/g) the adsorption capacity at equilibrium and C_e (g/L) the concentration of the adsorbate at equilibrium. Both the constants K_E and q_e are calculated from the plot of $\ln(q_e/C_e)$ vs q_e .

Adsorption isotherms were applied to evaluate the amount of adsorbate accumulation on the adsorbent surface and the type of interaction. The graphical representation of the linearized forms of the four models allowed us to calculate the constants of the different models (Table 3). The experimental equilibrium data evaluated by classical models, based on the R^2 coefficient as a criterion, show the applicability of the Langmuir and Temkin models with a maximum adsorption

capacity q_{max} (30.30 mg/g, $R^2 = 0.999$, at 25°C). The Langmuir model was best suited to fit the experimental data. Noted that R_L indicates the type of isotherm. In our case, the separation factor R_L takes values between 0.933 and 0.541 in the concentration range studied (10 - 120 mg/L) confirms that the adsorption is well described by the Langmuir isotherm which suggests one of the following three main hypotheses:

- (i) The adsorption sites have identical adsorption energy.
- (ii) The adsorbate occupies only one site on the surface.
- (iii) The adsorption is mostly confined to the adsorbent surface.

Influence of Temperature

Temperature is an important factor that influences the adsorption of solutes on the surface of activated carbons. Its importance is not limited only to the need to understand how it affects adsorption and desorption. The experimental results obtained allow access to the thermodynamic functions, which are evaluated from the modeling of the experimental results with adequate theoretical models. The variation of the adsorbed quantity q_{ads} the MB equilibrium as a function of temperature (10 °C–60°C), is illustrated in Figure 10.

Thermodynamic Properties Modeling Studies

The adsorption capacity of MB increases with temperature (20 °C–60°C), beyond which vaporization becomes problematic. The adsorption mechanisms can be determined from the thermodynamic functions: free energy (ΔG°), enthalpy (ΔH°) and entropy (ΔS°). The equilibrium constant (K) is calculated by Khan and Singh⁴⁵ by plotting $\ln(q_e/C_e)$ as a function of q_e and extrapolating to zero. The thermal effect on the adsorption of ACS has been studied between 293 and 313 K. The adsorption of MB involves a variation of the free energy ΔG° (kJ/mol) between the initial and final states which predicts the feasibility of the reaction:

$$\Delta G^\circ = \Delta H^\circ - T\Delta S^\circ \quad (14)$$

ΔG° is composed of the enthalpy term (ΔH°) which corresponds to the energies of interactions molecules/adsorbent, and entropic term (ΔS°) which expresses the modification and

Table 3. Constants of Isotherms Models (Adsorbent Dose: 8 g/L, Particle Size: 0.2 mm, pH: 6, Agitation Speed: 200 r/min, Time: 60 min, and T: 25°C).

25° C	Langmuir	Freundlich	Temkin	Elovich
K_L	0.00709 L/mg	$1/n : 0.738$	$B : 5.25$	$K_E : 0.0116$ L/mg
q_{max}	30.30 mg/g	$K_F : 0.406$ mg/g	$A_T : 0.112$ L/mg $\Delta Q : 10.012$ KJ/mol	$q_{max} : 20.00$ mg/g
R^2	0.999	0.989	0.989	0.989
X^2	0.234	1.750	1.875	2.012

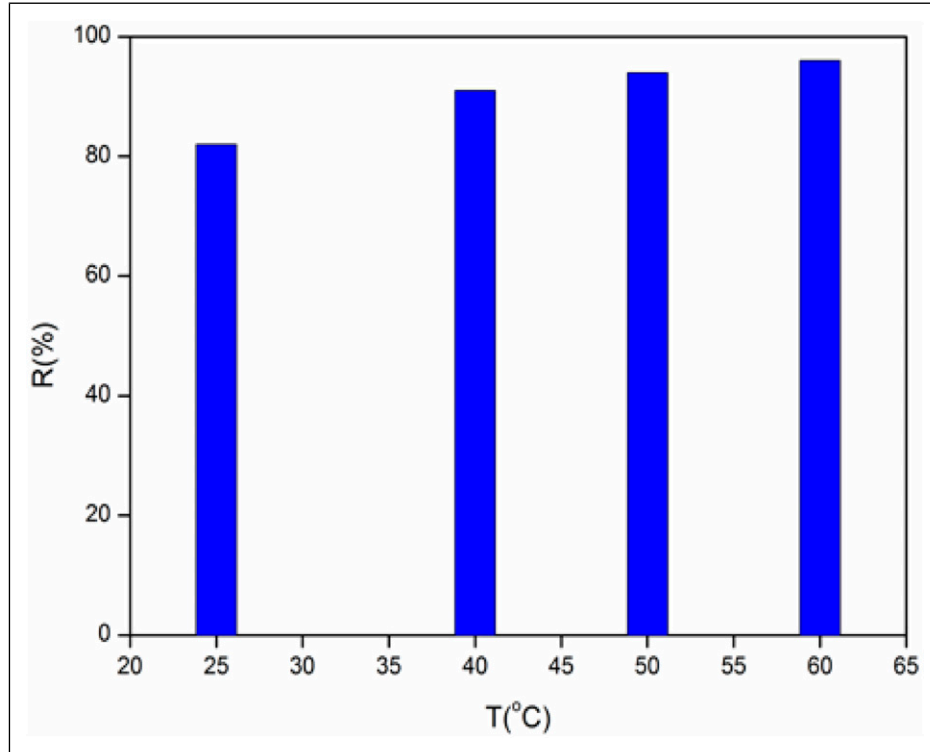


Figure 10. Effect of Temperature on the adsorption of MB onto ACS: (Adsorbent dosage: 8 g/L, Co: 10 mg/L, Particle size: 0.2 mm, pH: 6, Agitation speed: 200 r/min, time: 60 min).

arrangement of the molecules in the liquid phase and on the surface. The functions ΔG° , ΔH° , and ΔS° are obtained from the formula:

$$\Delta G^\circ = -RT \ln K_o \quad (15)$$

K_o is the apparent equilibrium constant; ΔH° and ΔS° are deduced from the intercept and slope of the line $\ln K_o$ vs $1/T$.

$$\ln K_o = -\frac{\Delta H^\circ}{RT} + \frac{\Delta S^\circ}{R} \quad (16)$$

The equilibrium constant (K_s) was calculated:

$$K_o = \frac{q_e}{C_e} \times \frac{\gamma_1}{\gamma_2} \quad (17)$$

γ_1 and γ_2 are respectively the activity coefficient of the adsorbed solute, and the solute in the equilibrium suspension. γ_1/γ_2 is assumed to be uniform for infinitely diluted solutions:

$$\lim_{C_e \rightarrow 0} \frac{q_e}{C_e} = K_o \quad (18)$$

The constant K_o is determined from intercept, by plotting $\ln(q_e/C_e)$ vs C_e and extrapolating to $C_e = 0$. The plot of $\ln K$ vs $1/T$ (Figure 11) is linear; the values of ΔH° and ΔS° are deduced from obtained from the graph (Equation (16)), the free enthalpy ΔG° at various temperatures are given in Table 4.

Note that the adsorbed MB amount with augmenting the temperature; this indicates that the adsorption is endothermic in nature (chemisorption).⁴⁶ The positive ΔG° (9.072 kJ/mol at 298 K to 0.196 kJ/mol at 334 K) value indicates a not spontaneous process while the positive ΔH° (82 kJ/mol) show that the MB adsorption on the ACS is endothermic, The entropy ΔS° (245.689 J/K.mol) with an increased randomness at the solid solution interface. As the adsorption time increases, the MB moves from a nearly ordered state to an disordered state within the solution, resulting in an increased rate of diffusion and removal.

Performance and Regeneration of the Adsorbent

It is instructive to compare the performance of some adsorbents available in the literature whose capacities are gathered in Table 5. We can see that the MB adsorption is well classified compared to other researches with a maximum adsorption capacity (q_{max}) of 30.30 mg/g, relatively interesting. The differences of the MB uptakes are due to the properties of each adsorbent namely the morphology, structure, functional groups and the surface area. ACS is an attractive adsorbent for dyes owing to the isoelectric point (pH_{pzc}). This study has yielded encouraging results, and we hope to extend the column adsorption to semi-pilot scale and test the photo-degradation of MB on semiconducting oxides is our next objective. Preliminary experiments have been satisfactory; the

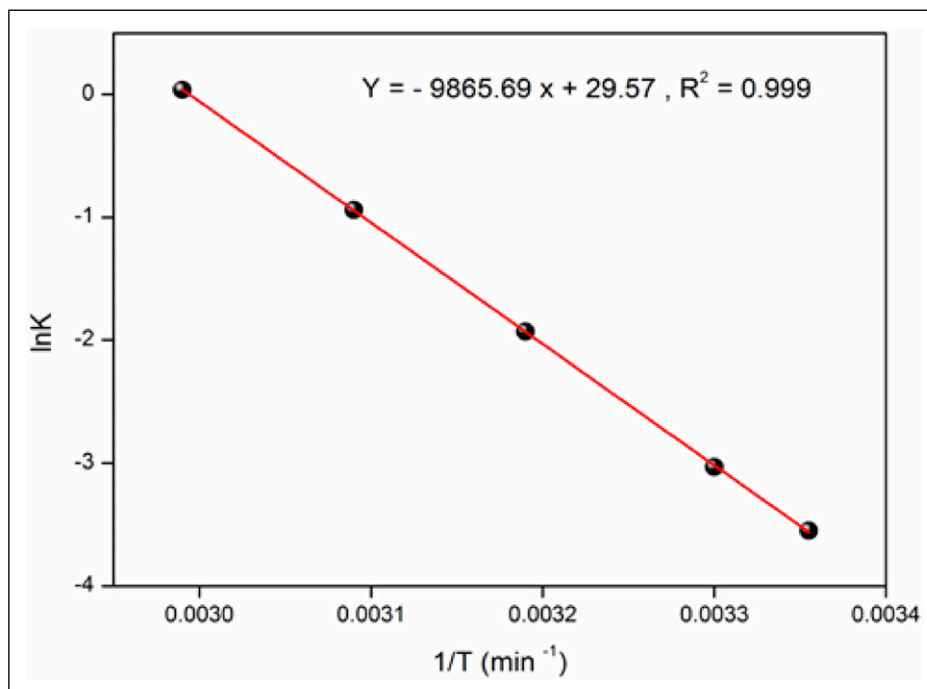


Figure 11. Linear form of $\ln K_d$ as a function of $1/T$ for MB adsorption onto ACS. (Adsorbent dose: 8 g/L, Co: 10 mg/L, Particle size: 0.2 mm, Agitation speed: 200 r/min, time: 60 min, and T: (25-60°C)).

Table 4. Determination of Thermodynamic Parameters (Adsorbent Dose: 8 g/L, Particle Size: 0.2 mm, pH: 6, Agitation Speed: 200 r/min, Time: 60 min, and T: (25 -60°C)).

T (K)	1/T (K ⁻¹)	K	Ln K	ΔG° (KJ/mol)	ΔH° (KJ/mol)	ΔS° (J/mol.K)
298	0.003355	0.029	-3.550	9.072	82.082	245.689
303	0.00330	0.048	-3.031	7.847		
313	0.00319	0.145	-1.932	5.395		
323	0.00309	0.390	-0.941	2.947		
334	0.00299	1.040	0.039	0.198		

tests are currently in progress and will be reported very soon.⁴⁷⁻⁶¹

The reusability of the adsorbent for further studies is important because it promotes cost-effectiveness and environmental friendliness.⁵⁷ It is essential to assess its ability to recover its initial efficiency after repeated cycles to extend its applicability on a large scale.⁵⁸ Regeneration avoids the use of new adsorbents, facilitates resource recovery and reduces both secondary waste generation and operational costs. The use of acidic solvents has been shown to be an effective desorption technique.^{59,60}

The choice of the solvent is essential for the recovery of adsorbates for further adsorptions and electrochemical, microbiological, thermal and chemical methods exist for this purpose. We opted for the chemical route because of its low cost where the regeneration of adsorbents for other cycles is economically important. The desorption of MB from ACS was evaluated using three solvents: H₂O, NaOH and HCl. The

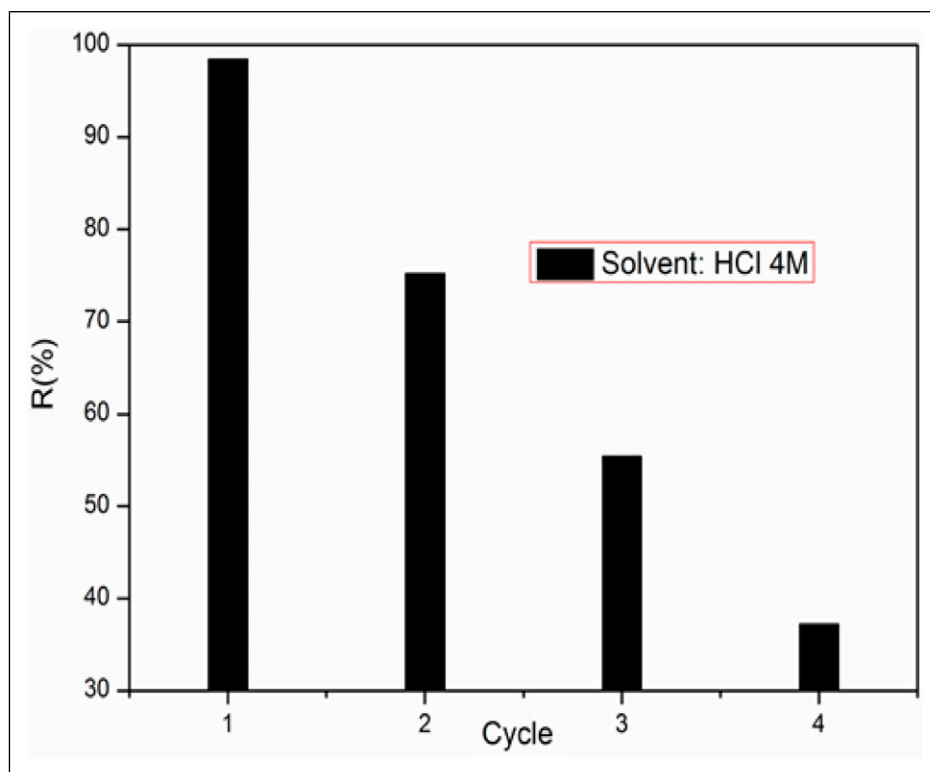
highest desorption was obtained in HCl solution (4 M) with a rate of 98.56% against 78.24% (NaOH) and 45.23% (H₂O). ACS was tested on 4 cycles ($R_1 = 98.56\%$, $R_2 = 75.26\%$, $R_3 = 53.25\%$ and $R_4 = 38\%$) (Figure 12). However, a gradual decrease in adsorption is observed from cycle 1 to cycle 4, attributed to the alteration of the surface structure of the adsorbent, thus leading to the blocking of several adsorption sites.

Adsorption Mechanism

As previously mentioned, the intraparticle diffusion is not the only factor limiting the MB adsorption onto ACS and other mechanisms can be involved simultaneously in the adsorption process of this system. In order to confirm the functional groups involved in the mechanism adsorption of MB, we compared the FTIR spectra of the activated carbon before and after the MB adsorption (Figure 1). The mechanism followed

Table 5. Comparative Study of the Maximum adsorption Capacity of MB Compared to the Bibliography.

Adsorbents	T (K)	Q_{max} (mg/g)	t_{eq} (min)	Dose (g/L)	pH	Ref.
Grounde palm kernel coat	298	277.771	60	60	9	49
Raw clay	298	50.012	50	0.2	10	50
Purified clay	298	65.512	50	0.2	10	50
Carbon Nano Tube	290	103.621	60	0.2	10	51
	300	109.310	60	0.2	10	51
	310	119.710	60	0.2	10	51
Strychnos potatorium	298	100.010	120	1	9	52
AC diatomaceous silica	298	126.601	120	1	9	53
Defatted <i>Carica papaya</i> seeds	298	769.231	70	1	10	54
Steam activated bituminous coal	298	580.000	60	0.05	11	55
Jute fiber carbon	298	225.650	50	1	10	56
Sawdust	293	142.360	50	1	7	57
Ccrushed brick	293	96.361	50	1	7	57
Apricot stone	298	46.031	35	1	10	58
	343	88.501	35	1	10	58
Zeolite	298	12.500	30	0.02	6	59
Rubber fruit shells	300	134.39	90	1	5	60
<i>Hevea brasiliensis</i>	298	90.504	60	5	8	61
Hydrogel composite	298	612.48	60	5	10	62
Chitosan	298	479.77	90	5	9	63
Upcycling of aquatic biota	298	3038.57	90	5	3	64
ACS	298	30.30	90	5	6	This study

**Figure 12.** Regeneration of the adsorbent (Adsorbent dose: 8 g/L, C_0 : 10 mg/L, Particle size: 0.2 mm, Agitation speed: 200 r/min, time: 60 min, and T: 25°C).

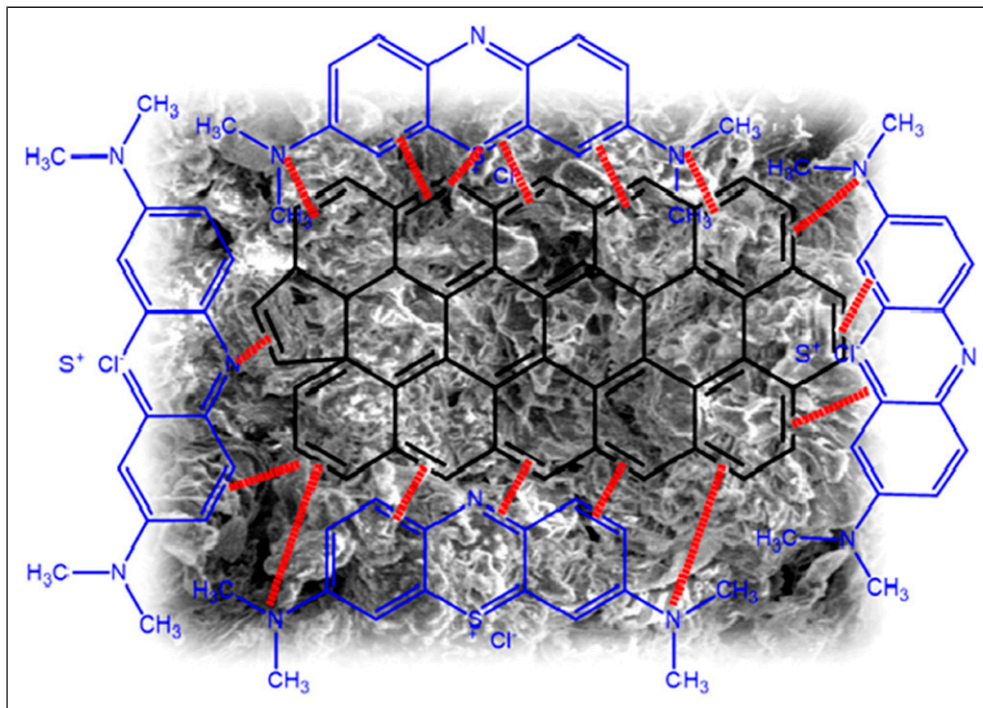


Figure 13. Adsorption mechanism.

in the removal of MB on ACS is shown in Figure 13. It includes π - π stacking, hydrogen bonding and electrostatic interaction. ACS has a positive charge at $\text{pH} < \text{pH}_{\text{pzc}} (=5.05)$, on its surface promoting the attraction of the anionic dye. For $\text{pH} > \text{pH}_{\text{pzc}}$, ACS acquires a negative charge on its surface, thus attracting electrostatically the cationic dye MB. The hydroxyl groups present on the ACS surface are involved in the hydrogen bond with the N, S, O atoms of MB and this is evident from the FT-IR results: the broad hydroxyl peak in ACS decreased after adsorption due to the involvement of $-\text{OH}$ groups in the adsorption mechanism. Furthermore, adsorption is promoted by π - π interactions between the ACS and the aromatic rings of MB. All these mechanisms facilitate the adsorption process on the surface of the adsorbent.

Examination of the IR spectra after adsorption confirms the fixation of MB on the surface of ACS. Indeed, we note the appearance of three bands assigned to the $\text{O}-\text{H}$, $\text{C}=\text{C}$ and $\text{C}-\text{O}$ groups where the increase in their intensity confirms the MB adsorption. The position of these bands is shifted, reflecting the existence of notable interactions between the MB molecules and the active sites of the carbon (Figure 13). The shift of the $\text{O}-\text{H}$ band confirms the formation of a hydrogen bond between MB and ACS. A hydrogen bond has occurred between the H-donor atoms and the acceptor groups on the surface of ACS.

The characteristic band of the aromatic group $\text{C}=\text{C}$ is shifted, reflecting the presence of hydrophobic interactions of π - π type, between the electron donor group π of the aromatic ring and the acceptor group on the ACS surface. The characteristic $\text{C}-\text{O}$ absorption band is also shifted compared to that

of native ACS, attesting to the strong n - π type interactions involved between the oxygenated groups of ACS as electron donor, and the aromatic ring.

Conclusion

The current study showed that ACS can be effectively used as a raw material for the preparation of activated carbon for MB dye removal. The Langmuir model provided a better fit to the equilibrium adsorption data with a maximum capacity of 30.30 mg/g at 25°C. The adsorption follows a pseudo-second-order kinetic model, where the chemisorption is the rate-limiting step. MB molecules are attached to the adsorbent surface by forming a chemical bond and tend to find sites that maximize their coordination number with the surface.

The kinetic and thermodynamic data were explored in detail for the design of real effluent treatment. The positive free enthalpy ΔG° and positive enthalpy ΔH° showed that the adsorption of MB on ACS is endothermic and non-spontaneous over the temperature range studied. The positive entropy ΔS° indicates a random character increases at the solid-solution interface during adsorption where a structural exchange can occur between the active sites of the adsorbent and the ions.

For a comparative study, it was instructive to give the adsorption capacity with the literature. We found that the uptake capacity of MB observed in the present work is well positioned compared to other adsorbents. The reusability of the adsorbent for further studies is a key consideration as it promotes cost-effectiveness and environmental friendliness.

This mini-batch study has yielded encouraging results, and we aim to perform the adsorption in column mode under the conditions applicable to effluent treatment at semi-pilot scale and the present study has shown that ACS is a potentially attractive adsorbent. The removal of MB in column mode and the degradation of the dye by heterogeneous photocatalysis will be our next step.

Abbreviation

Nomenclature

MB	Methylene blue
ACS	Activated Coconut Shells
FTIR	Fourier Transform Infrared spectroscopy
pHpzc	point of zero charge
R_L	Separation factor
ΔG° (kJ/mol)	Free energy
ΔS° (J/K.mol)	Entropy
ΔH° (kJ/mol)	Enthalpy
C.I	Index Color
λ_{max}	Absorbance peaks
R (%)	Elimination yield
q_t (mg/g)	The adsorbent quantities
R^2	Determination coefficient
X^2	Chi-Squares
V	The volume
C_o	The initial concentration
N	The number of observations
$q_{e(exp)}$ (mg/g)	The experimental value
$q_{e(cal)}$ (mg/g)	The calculated value
SEM	Scanning Electron Microscope
t (s)	Time
k_1 (min ⁻¹)	The rate constant in the pseudo-first-order model
k_2 (g/mg min)	The pseudo second order rate constant
α (mg/g min)	The initial adsorption rate
β (mg/g)	Relates the degree of surface coverage
K_{in} (mg/gmin ^{1/2})	The intra-particle diffusion rate
C	The thickness of the boundary layer
K_L (L/mg)	Langmuir constant
K_F (L/mg)	Fruendlich constant
K_E (L/mg)	Elovich constant
A_T and B_T	The Temkin constants
n :	related rto the capacity of favorability of adsorption
ΔQ (J/mol)	The Temkin energy change
q_{max} (mg/g)	The maximum adsorption capacity
T (K)	Temperatuze
γ_1 and γ_2	The respectively the activity coefficient

Author Contributions

Pr. Moussa ABBAS conceived and designed the study, performed the experiments and analyzed the data. And Pr. Mohamed Trari revise

and correction of the manuscript. All authors reviewed and approved the final version of the manuscript.

Declaration of Conflicting Interests

The author(s) declared no potential conflicts of interest with respect to the research, authorship, and/or publication of this article.

Funding

The author(s) disclosed receipt of the following financial support for the research, authorship, and/or publication of this article: This work was supported by the laboratory of Applied Chemistry and Materials (LabCAM), University of M'hamed Bougara of Boumerdes, Avenue de l'Indépendance Boumerdes, 35000, Algeria.

CRedit Authorship Contribution Statement

M. Abbas: investigation, writing original draft, formal analysis; interpretation of results;

M. Trari: investigation; interpretation of results; Supervision; conceived the idea and supervision, writing review and editing.

ORCID iD

Moussa Abbas  <https://orcid.org/0000-0002-0420-2414>

Data availability statement

All data presented in this study are included in the manuscript by the corresponding author.

References

- Vakili M, Rafatullah M, Ibrahim MH, Abdullah AZ, Salamatinia B, Gholami Z. Oil palm biomass as an adsorbent for heavy metals. *Rev Environ Contam Toxicol.* 2014;232:61-88.
- Alok M. A review on halloysite-based adsorbents to remove pollutants in water and wastewater. *J Mol Liq.* 2018;269:855.
- Charu A. Iron based metal organic framework for efficient removal of methylene blue dye from industrial waste. *J Mol Liq.* 2019;284:343.
- Sanju S. Utilisation of cobalt doped Iron based MOF for enhanced removal and recovery of methylene blue dye from waste water. *J Mol Liq.* 2020;314:113642.
- Ioannis AP. Removal of caffeine, nicotine and amoxicillin from (waste) waters by various adsorbents. A review. *J Environ Manag.* 2020;261:110236.
- Vinod KG. Sequestration of toxic Congo red dye from aqueous solution using ecofriendly guar gum/ activated carbon nanocomposite. *Int J Biol Macromol.* 2020;158:1310.
- Connor R. *The united nations world water development report. Wastewater: the untapped resource.* The United Nations World Water Development Report; 2017.
- Gupta VK, Mittal A, Krishnan L, Gajbe V. Adsorption kinetics and column operations for the removal and recovery of malachite green from wastewater using bottom ash. *Sep Purif Technol.* 2004;40:87-96.

9. Mittal A, Mittal J, Malviya A, Gupta VK. Adsorptive removal of hazardous anionic dye Congo red from wastewater using waste materials and recovery by desorption. *J Colloid Interface Sci.* 2009;340:16-26.
10. Mittal J. Permissible synthetic food dyes in India. *Reson.* 2020; 25(4):567-577.
11. Raval NP, Shah PU, Shah NK. Malachite green a cationic dye and its removal from aqueous solution by adsorption. *Appl Water Sci.* 2017;7:3407-3445.
12. Ghasemi M, Mashhadi S, Asif M, Tyagi I, Agarwal S, Gupta VK. Microwave-assisted synthesis of tetra ethylene pentamine functionalized activated carbon with high adsorption capacity for Malachite green dye. *J Mol Liq.* 2016;213:317-325.
13. Abbas M. Experimental 2020 .investigation of activated carbon prepared from apricot stones material (ASM) adsorbent for removal of malachite green (MG) from aqueous solution. *Adsorpt Sci Technol*;38(1–2):24.
14. Abbas M, Harrache Z, Trari M. Mass-transfer processes in the adsorption of crystal Violet by activated carbon derived from Pomegranate peels: kinetics and thermodynamic studies. *J. Eng. Fibers Fabr* 2020;15(1):155892502091984.
15. Abbas M. Performance of Apricot Stone to remove dyes from aqueous solutions –Equilibrium, kinetics, isotherms modeling and thermodynamic studies. *Mater Today Proc.* 2020;31: 437-443.
16. Abbas M. Experimental investigation of titanium dioxide as an adsorbent for removal of Congo red from aqueous solution, equilibrium and kinetics modeling. *J. Water Reuse Desal* 2020; 10(3):251-266.
17. Abbas M. Removal of methylene blue (MB) in aqueous solution by economic adsorbent derived from apricot stone activated carbon (ASAC). *Fiber. Polym.* 2020;21:810. No4.
18. Abbas M, Harrache Z, Trari M. Removal of Gentian Violet in aqueous solution by activated carbon equilibrium, kinetics, and thermodynamic study. *Adsorpt Sci Technol.* 2019;37(7–8): 566-589.
19. Abbas M, Aksil T, Trari M. Removal of toxic methyl green (MG) in aqueous solutions by apricot stone activated carbon - equilibrium and isotherms modeling. *Desal. Wat. Treat.* 2018; 125:93-101.
20. Merrad S, Abbas M, Trari M. Adsorption of malachite green onto Walnut shells: kinetics, thermodynamic, and regeneration of the adsorbent by chemical process. *Fibers Polym.* 2023;24: 1067-1081.
21. Arora C, Soni S, Sahu S, Mittal J, Kumar P, Bajpai P. Iron based metal organic framework for efficient removal of methylene blue dye from industrial waste. *J Mol Liq.* 2019;284:343-352.
22. Soni S, Bajpai P, Mittal J, Arora C. Utilisation of cobalt doped Iron based MOF for enhanced removal and recovery of methylene blue dye from waste water. *J Mol Liq.* 2020;314: 113642.
23. Harrache Z, Abbas M. Elimination of a cationic dye in aqueous solution by adsorption on activated carbon: optimization of analytical parameters, modeling and thermodynamic study. *Journal of Engineered Fibers and Fabrics.* 2022;17:1-12.
24. Jawad AH, Rashid RA, Ismail K, Sabar S. High surface area mesoporous activated carbon developed from coconut leaf by chemical activation with H₃PO₄ for adsorption of methylene blue. *Desalination Water Treat.* 2017;74:326-335.
25. Ali HJ. Conversion of Malaysian low-rank coal to mesoporous activated carbon: structure characterization and adsorption properties. *Chin J Chem Eng.* 2019;27:1716.
26. Ali HJ. Zwitterion composite chitosan-epichlorohydrin/zeolite for adsorption of methylene blue and reactive red 120 dyes. *Int J Biol Macromol.* 2020;163:756.
27. Paz A, Carballo J, Pérez MJ, Domínguez JM. Biological treatment of model dyes and textile wastewaters. *Chemosphere.* 2017;181:168-177.
28. BuhaniIstikomah, Suharso. Cationic Surfactant modified Tetraselmis sp. for the removal of organic dyes from aqueous solution. *Molecules.* 2023;28(23):7839.
29. Khan ZA, Elwakeel KZ, Mashabi RA, Elgarahy AM. Adsorption of anionic dyes onto 1, 5-Diphenylcarbazine functionalized magnetic hybrid polymer: Impact of water salinity and surfactants on adsorption isotherms. *J Ind Eng Chem.* 2024;131:569-584.
30. Raed A. Chitosan- or glycidyl methacrylate-based adsorbents for the removal of dyes from aqueous solutions: a review *Mater. Adv.* 2022;3:5645-5671.
31. Elwakeel KZ. Removal of Reactive Black 5 from aqueous solutions using magnetic chitosan resins. *J Hazard Mater.* 2009; 167:383-392.
32. Maalej-K. Malachite green decolourization and detoxification by the laccase from a newly isolated strain of *Trametes* sp. *Int. Biodeterio. Biodegradation.* 2009;63:600.
33. Abbas M, Trari M. Photocatalytic degradation of AsucryL Red (GRL) in aqueous medium on heat-treated TiO₂ powder - effect of analytical parameters and kinetic modeling. *Desal. Water Treat.* 2020;180:398-404.
34. Abbas M, Trari M. Contribution of adsorption and photo catalysis for the elimination of Black Eriochrome (NET) in an aqueous medium-optimization of the parameters and kinetics modeling. *Scientific African.* 2020;8:00387.
35. Gao R, Hu Z, Chang X, et al. Chemically modified activated carbon with 1- acylthiosemicarbazide for selective solid-phase extraction and preconcentration of trace Cu (II), Hg (II) and Pb (II) from water samples. *J Hazard Mater.* 2009;172:324-329.
36. Hu L, Peng Y, Wu F, Peng S, Li J, Liu Z. Tubular activated carbons made from cotton stalk for dynamic adsorption of airborne toluene. *J Taiwan Inst Chem Eng.* 2017;80:399-405.
37. Lagergren S. *Kung* 1898, about the theory of So-called adsorption of soluble substances. *Sven. Vetenskapsakad Handingargl*;24:1-39.
38. Ho YS, McKay G. Kinetic models for the sorption of dye from aqueous solution by wood. *Process Saf Environ Prot.* 1998; 76(4):183-191.
39. Juang RS, Chen ML. Application of the Elovich equation to the kinetics of metal sorption with solvent-impregnated resins. *Ind Eng Chem Res.* 1997;36:813-820.
40. J weber M, Morris J. Kinetic of adsorption on carbon from solution ASCE. *Journal Saint Engineering Division.* 1963;89:31.

41. Langmuir I. The adsorption of gases on plane surface on glass, mica and platinum. *J Am Chem Soc.* 1918;40(9): 1361-1403.
42. Freundlich H. Concerning adsorption in solutions. *Z. Phys. Chem. Stoch.* 1906;57:385-470.
43. Temkin M, Pyzhev V. Kinetics of ammonia synthesis on promoted iron catalysts. *Acta Physicochim URSS.* 1940;12:327-356.
44. Abbas M. Removal of amoxicillin from wastewater onto activated carbon: optimization of analytical parameters by response surface methodology, dose-response. *Int J.* 2024: 1-15.
45. Khan AA, Singh RP. Adsorption thermodynamics of carbofuran on Sn (IV) arsenosilicate in H⁺, Na⁺ and Ca²⁺ forms. *Colloid Surface.* 1987;24(1):33-42.
46. Oladoja NA. Kinetic and isotherm studies of Methylene Blue adsorption onto ground palm kernel coat. *Turkish J. Eng. Environ. Sci.* 2008;V32:303.
47. Bennani A. Removal of basic dye Methylene Blue in aqueous solution by Safi clay. *J Water Sci.* 2010;23(N4):375.
48. hardryari Z. Experimental study of Methylene Blue adsorption from aqueous solution onto nanotube. *Int. J. Water Res. Environ. Eng.* 2010;2:16-28.
49. Jerald Antony M. Equilibrium isotherm studies of Methylene Blue from aqueous solution onto activated carbon prepared from strychnos potatorium seed. *Int. J. Appl. Biol. Pharma Technol.* 2012;3:27.
50. Al-Qodah Z, Lafi W, Al-Anber Z, Al-Shannag M, Harahsheh A. Adsorption of Methylene Blue by acid and heat treated diatomaceous silica. *Desalination.* 2007;217:212-224.
51. Emmanuel I. Multistage optimization of the adsorption of Methylene Blue dye onto defatted Carica papaya seeds. *Chem. Eng. J* 2009;V155:567-579.
52. Emad NEIQ. Adsorption of Methylene Blue onto activated carbon produced from steam activated bituminous coal: a study of equilibrium adsorption isotherm. *Chem. Eng. J.* 2006; 124(1-3):103-110.
53. Senthil Kumar S, Varadarajan PR, Porkodi K, Subbhuraam CV. Adsorption of Methylene Blue onto jute fiber carbon: kinetics and equilibrium studies. *J Colloid Interface Sci.* 2005;284(1): 78-82.
54. Hamdaoui O. Batch study of liquid-phase adsorption of Methylene Blue using cedar sawdust and crushed brick. *J Hazard Mater.* 2006;135(1-3):264-273.
55. Abbas M, Trari M. Removal of methylene blue in aqueous solution by economic adsorbent derived from apricot stone activated carbon. *Fibers Polym.* 2020;21(N4):810-820.
56. Abbas M. Removal of Methylene Blue (MB) pollutant from the textile industry by adsorption onto zeolite Kinetic and thermodynamic study. *Journal of Engineered Fibers and Fabrics.* 2022;17:1-11.
57. Osman AI, El-Monaem EMA, Elgarahy AM, et al. Methods to prepare biosorbents and magnetic sorbents for water treatment: a review. *Environ Chem Lett.* 2023;21:2337-2398.
58. Ma H, Zhang XF, Wang Z, Song L, Yao J. Flexible cellulose foams with a high loading of attapulgite nanorods for Cu²⁺ ions removal. *Colloids Surf A Physicochem Eng Asp.* 2021;612: 126038.
59. Vakili M, Gholami F, Zwain HM, et al. Treatment of As(III)-contaminated food waste using alkali treatment and its potential application for methylene blue removal from aqueous solutions. *J Water Process Eng.* 2023;55:104100.
60. Vakili M, Deng S, Cagnetta G, et al. Regeneration of chitosan-based adsorbents used in heavy metal adsorption: a review. *Sep Purif Technol.* 2019;224:373-387.
61. Khalid Z. Biogenic tunable sorbent produced from upcycling of aquatic biota-based materials functionalized with methylene blue dye for the removal of chromium (VI) ions. *J Environ Chem Eng.* 2021;9:104767.